Proceedings of 8 ICSHMO, Foz do Iguaçu, Brazil, April 24-28, 2006, INPE, p. 627-632.

GRAVITY WAVE GENERATION AND BREAKING OBSERVED WITH RADIOSONDES AT USHUAIA (ARGENTINA)

Manuel Pulido(+) and Hector Teitelbaum(*)
(+) Facultad de Ciencias Exactas y Naturales
Universidad Nacional del Nordeste
Av. Libertad 5460, (3400) Corrientes, Argentina.
pulido@exa.unne.edu.ar
(*) Laboratoire de Meteorologie Dynamique
Ecole Normale Superieure
24 Rue Lhomond 75235 Paris Cedex 05 France
teitel@lmd.ens.fr

Abstract

High resolution radiosondes that were launched at Ushuaia (54.8S) during October-December, 1995 are examined. Episodes of high gravity wave activity are found in the lower stratosphere (from 10 km to 24 km). The enhancement of gravity wave activity is ascribed to the conjuction of two factors: gravity wave generation and Doppler-shifting. Two radiosondes with high wave activity cases are examined. They present inertio-gravity waves (IGW) with horizontal wavelengths of 400-700 km. Profiles of the Richardson number (Ri) present some patches where Ri descends bellow one quarter mainly induced by wave shear. These patches are identified as regions where IGWs are breaking. The possibility of gravity wave generation by orography and geostrophic adjustment are evaluated using the synoptic situation from ECMWF analyses and WRF simulations. We argue that synoptic waves propagating eastward over the Andes mountain range are generating the high wave activity events.

1. INTRODUCTION

The weaker planetary wave activity observed in the southern hemisphere compared to the northern hemisphere is believed to be mainly due to the lack of land-sea contrast. The strong nocturnal jet found in the middle atmosphere is a result of this weak planetary wave activity. Garcia and Boville (1994) have shown that gravity waves may play a major role in the middle atmosphere flow of the southern hemisphere, they note that gravity wave drag compensates the lack of planetary wave drag, producing important dynamical effects as low as 20 km trough the so-called downward control principle.

Gravity waves may have also an important role in constituent mixing within the polar night jet. The coupling of inertio gravity waves with the large-scale flow only taking into account linear propagation results in a cross-jet mixing (Pierce, *et al.* 1994). However nonlinear processes are expected to have the major effect, nonlinear inertio-gravity waves could affect the permeability through the strong isentropic potential vorticity gradient found in the southern stratospheric vortex (McIntyre 1989).

In the troposphere, the southern hemisphere jet-stream descends to very low heights; the longitudinally and seasonally averaged zonal wind has a peak at 50S of almost 10 m/s (Holton 1992, p143) , gusts may increase this value by a factor of 4. This particular behaviour is not found in the Northern Hemisphere. These strong surface winds are usually present in South America, in the Patagonia region, a place particularly suitable for wind power generation. Figure 1 shows zonal winds at 850 hPa averaged from September to November from ECMWF ERA40 Atlas, the strong low tropospheric jet is the prevailing feature in this map. As the tropospheric jet-stream reaches South America, it finds the Andes mountain range, so gravity wave generation by orography is highly probable on the lee side of the Andes between 45S and 55S.

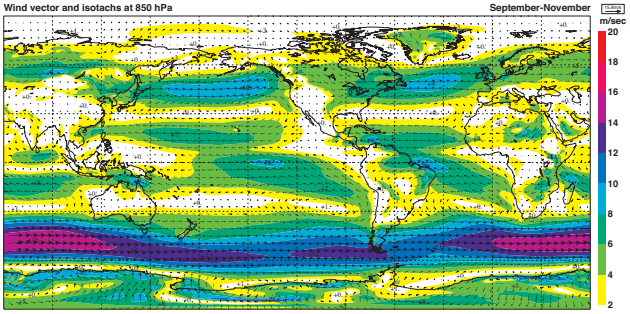

Figure 1:Vector wind at 850 hPa (~1 km) from ERA40 Atlas (ERA40 data temporally averaged from 1979 to 2001) for the September to November period.

The maximum time averaged zonal winds are regions where synoptic waves tend to develop and to propagate downstream along the so-called storm tracks. The zonal wind jet in Fig. 1 coincides with the region where the South Pacific storm tracks are located (Trenberth 1991, Orlanski and Katzfey, 1991). Note that the development of these synoptic waves should not be associated with the horizontal shear but with the zonal wind vertical shear which is present in those regions. Indeed synoptic waves has been shown to owe their existence to the baroclinicity of the large-scale flow (Charney, 1947).

The development of baroclinic waves is an important source of inertia-gravity waves (O'Sullivan and Dunkerton, 1995). The baroclinic wave development produces a distortion in the tropospheric jet-stream, the flow is then adjusted toward geostrophic balance from the unbalanced state triggering inertia-gravity waves. This will occur mainly in the exit region of the jet-stream

where the unbalance is more marked, as has been found in observations (Uccellini and Koch, 1987).

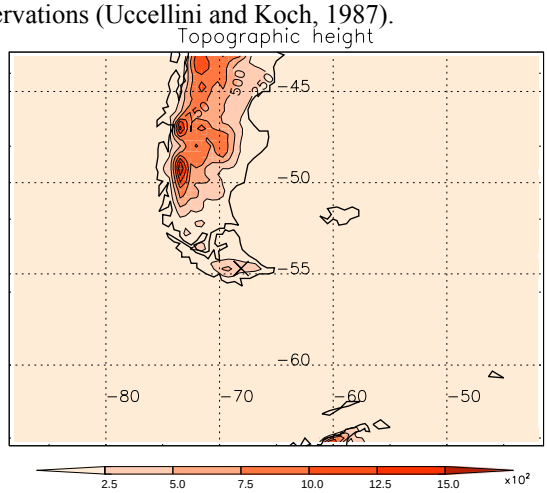

Figure 2. Topographic height [m] in the region of the WRF simulations. Crosses show the two sites chosen to analyse profiles (at the lee side of the main mountain and at Ushuaia).

In this work we examine a series of radiosondes that were released at Ushuaia, Argentina. The launching site presents ideal conditions to analyse gravity wave generation mechanisms, orography and geostrophic adjustments are both expected to be mayor sources of waves at that site as argued above. In particular, Ushuaia is located to the East of The Andes mountain range. Figure 2 shows the topographic heights (Ushuaia is marked with a cross). Apart the 800 m mountain located to the west, the over 1600 m mountains located to the northwest will have a central role in orographic generation as we will see in what follows. Furthermore the other aspect necessary for orographic wave generation, surface winds, is guaranteed in that region, where strong winds are present almost all the year around. The radiosonde analysis is presented in Section 2.

For the strongest wave event we performed a numerical simulation with the Weather and Research Forecast (WRF) model, using ECMWF reanalysis data as initial and boundary conditions. Previous studies have shown that WRF is a useful tool to examine gravity wave generation from ideal conditions (Zhang, 2004) and from reanalysis data. Besides, ECMWF data are not only suitable as initial and boundary conditions for these wave generation experiments. Signatures of these kind of waves appear to be visible in the data and with similar characteristics to in-situ measurements (Plougonven and Teitelbaum, 2003). Results of the numerical experiments can be found in Section 3.

2. DATA ANALYSIS

A series of radiosondes were launched by the Centre National d'Etudes Spatiales (CNES, France) at Ushuaia, Argentina (54.7S, 68.1W) from 10/25/1995 to 12/12/1995. The purpose of this short campaign was to investigate stratospheric vortex breaking previous to STRATEOLE/VORCORE campaign.

The height range covered by radiosonde goes from ground to about 30 km. Measurements were made with a time step of 10 s which implies a vertical resolution of about 50 m. The points are equispaced in height using a cubic spline technique with a vertical resolution of 40 m. If an outlier point is detected, it is rejected and its value is replaced by an interpolation between neighbour points.

The wind perturbation is calculated using a low-pass filter (Scavuzzo *et al.*, 1998). We identify wavelengths greater than 8 km as the background wind, perturbations with wavelengths between 800m and 8 km are taken as the wave field. Before filtering we performed a wavelet analysis which show that the main disturbance have a vertical wavelength of 4 km as we will discuss next.

Assuming quasi-horizontal motions (zonal and meridional wind perturbations, u',v', much greater than vertical wind perturbations, w'), the wave energy per unit mass is given by,

$$E = \frac{1}{2}\left[\overline{u'^2} + \overline{v'^2} + \frac{g^2}{\overline{N}^2}\overline{\left(\frac{T'}{\overline{T}}\right)^2}\right]$$

where T' is the temperature perturbation, T is the height-dependent background temperature, and N is the (background) Brunt Vaisala frequency. Spatial averaging is denoted by overbars.

Figure 3 shows the wave energy per unit mass in the stratosphere (heights greater than 12 km) as a function of the day of the year, the wave field is highly variable with peaks of wave energy that exceed 8 J/kg, in other words the height-averaged amplitude of zonal/meridional wind perturbation are above 2 m/s in the high wave activity profiles (locally they reach values of 10 m/s). Our interest is in analysing the wave source of the high wave activity episodes, in this preliminary analysis we will focus in one of these events.

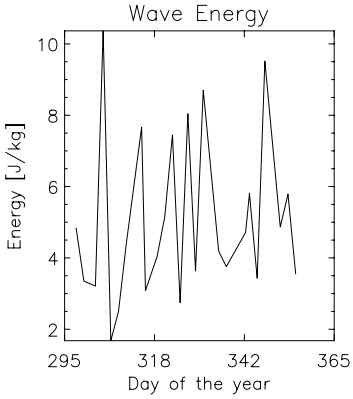

Figure 3: Wave energy per unit mass as a function of day of the year.

Further analysis is performed to the radiosondes launched on 10/30 and 11/01, the last one presents the highest stratospheric wave energy during the observation period. Figure 4 shows the zonal and meridional wind. There is a strong southward wind which is maximum at 12 km, aloft there is a strong shear region where gravity wave activity increases. On 11/01, Fig. 5 shows a highly perturbed profile, the zonal background wind reaches 50 m/s at 12 km and diminishes aloft, at 35 km is zero. The intensity of the meridional background wind is also maximum at 12 km in which it reaches 35 m/s, the meridional wind is zero at 25 km.

The wind perturbations, Fig. 6, present highest activity just above the tropopause (at ~9 km) in both measurements (10/30 and 11/01). It is evident that the disturbance is starting to develop on 10/30 and remains and enhances on 11/01. In the troposphere the meridional

and zonal components are in phase, the vertical wavelength exceeds 8 km. In the stratosphere the perturbation field exhibits different characteristics, the vertical wavelength is much shorter (~4 km) and the components are out of phase suggesting in principle the presence of inertia gravity waves with intrinsic periods near the inertial period. The perturbations diminish abruptly above 27 km, also note that the wavelength is shortening as the wave propagates towards that height, there probably a critical layer may be developing. The filtering window used to obtain the perturbations shown in Fig. 6 is 2-13 km, this long window keeps all the information of the perturbation including the strong refraction that the wave field is suffering.

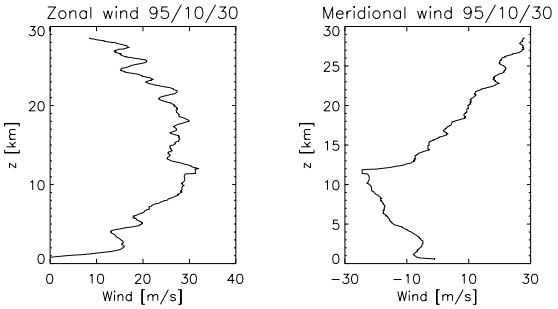

Figure 4: Zonal (left panel) and meridional (right panel) wind profiles measured on 10/30.

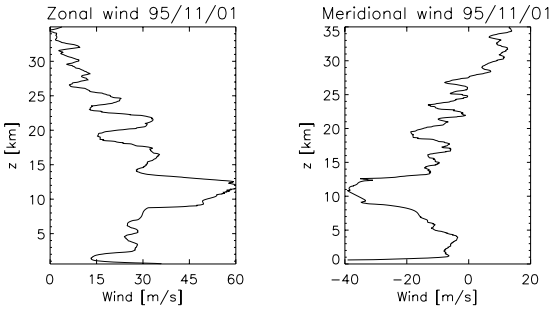

Figure 5: As Fig. 4 on 11/01.

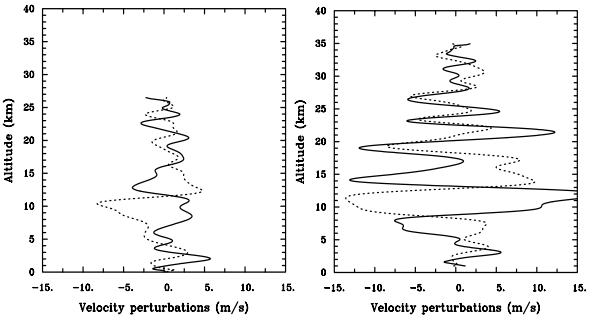

Figure 6: Zonal (continuous line) and meridional (dotted line) wind perturbations obtained with a filtering window of 2-13 km on 10/30 (left panel) and 11/01 (right panel).

Figure 7 shows a wavelet analysis of the zonal wind on 11/01, the disturbance is dominated by a vertical wavelength of 4.5 km, the waves are refracted towards shorter wavelength as they propagate upward, suggesting again the presence of a critical level above 27 km. Regrettably, the wavelet technique is unable to determine the wavelength near the extremes of the interval, so that the troposphere is not represented. The tendance suggests tropospheric wavelengths greater than 7 km. The meridional wind (Fig. 7 left panel) also shows clearly a perturbation of 4 km of wavelength, the refraction is not evident. The wavelet analysis justifies the 2-13km filtering window used to produce the wind perturbation profile in Fig. 6.

The stratospheric hodographs are shown in Fig. 8. They are showing an elliptical polarisation. The wave propagation direction is northwest-southeast on 10/30 and southwest-northeast on 11/1. In principle the ellipticity of the hodograph must be the signature of inertia-gravity waves with intrinsic periods near the inertial period. If the observed waves were generated by the mountains located at the west of Ushuaia we would expect a linear polarisation in the west-east direction.

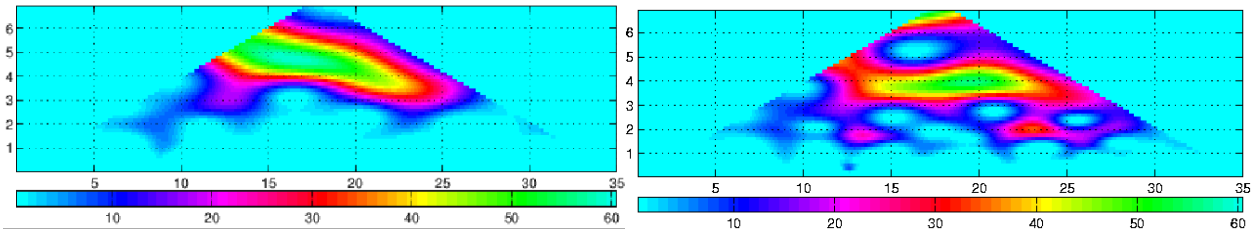

Figure 7: Wavelet analysis of the zonal wind profile (left panel) and meridional wind (right panel) on 11/01. X-axis height (km) and y-axis wavelength (km).

Similar perturbation characteristics have been found in other observational studies, however there is no a unique interpretation. Hines (1989) argues that a component perpendicular to the wave propagation direction is induced by the shear, therefore an elliptical polarisation is expected when the waves are propagating in strongly sheared environments. Cornish and Larsen (1989) propose that the orographic source may be modulated by the diurnal fluctuation of the surface winds generating waves with small intrinsic frequencies. Scavuzzo *et al.* (1998) suggest another interpretation of this inertio-gravity waves observed above orography, they may be triggered by the geostrophic adjustment of the flow which is in an unbalanced state produced by the presence of the linear/nonlinear orographic waves. The preliminary results presented here do not allow us to discern between these interpretations, further investigation will be carry out to shed light on the sources of the inertia-gravity waves observed over Ushuaia.

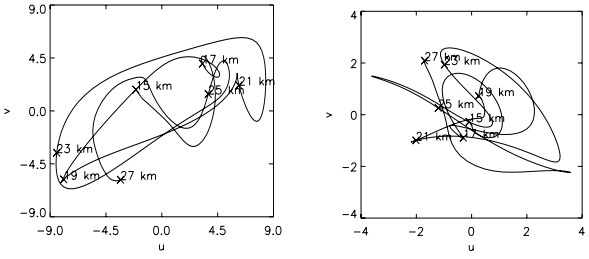

Figure 8: Hodograph for the wind perturbation (800m-

8km) on 10/30 (left panel) and on 11/01 (right panel). Marks show corresponding heights of the wind points.

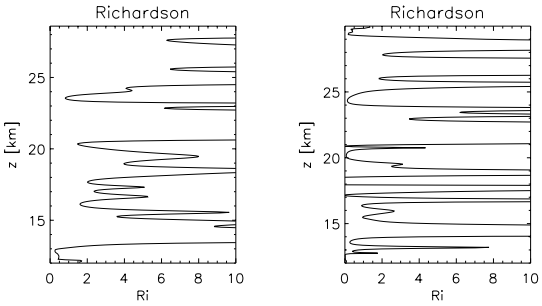

Figure 9. Richardson number for the total flow (800 m low-pass filtered) on 10/30 (left panel) and on 11/01 (right panel).

Figure 9 shows the Richardson number, to calculate it, we filter the fields with 800 m low-pass filter. On 10/30 the Ri profile shows that the flow is stable dynamically with a Ri greater than one, except in the lowest heights where a burst in the wind produces a patch of small Richardson number. On 11/01, the wave field is clearly unstabilizing the flow in several patches, some of them present dynamical instabilities while others present convective instabilities suggesting that the wave field is breaking.

3. WRF SIMULATIONS

To investigate further the generation and breaking mechanisms of the high activity wave events, which are not clear from radiosonde analysis, we performed numerical simulations using the WRF model and ERA 40 analysis data (ECMWF) as initial and lateral boundary conditions. The domain is shown in Fig. 2, it is centred near Ushuaia and has an extension of 3000 km in longitude and 2400 km in latitude with a horizontal resolution of 30 km and a vertical resolution of 400 m. The model was started on 10/30 00UTC (we compared it with a simulation started from 10/25, there were no visible differences).

3.1 Wave generation

The impact of the Andes mountain range on the gravity wave generation was assessed by means of a simulation with the same conditions as the control run but without orography. The wave patterns observed in every field dissappear in this ``flat'' simulation. There were no signs of the waves during the whole simulation.

Figure 10 shows the evolution of the wave pattern at 16 km for 10/30 (after 12 hours of simulation), 10/31, 11/1 at 12:00UTC. It is clear how the wave pattern is generated over the orography and then wave packets propagate southeastward. The horizontal wavevector appears to be oriented to the East. The wavelength is about 400 km, but it is changing with time, note the very long wavelengths present on 10/31 (about 700 km). On 11/1, the day of the second radiosonde (Fig. 5), the disturbance is mainly located over Tierra del Fuego island. Both, horizontal wavelength changes and wave propagation appears to be dominated by the strong horizontal shear found in the region.

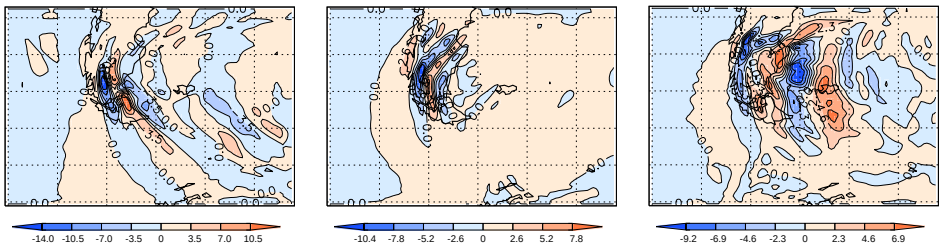

Figure 10: Evolution of the wave pattern at 16 km on 10/30 (left panel), 10/31 (middle panel) and 11/1 (right panel) obtained from zonal wind differences between with and without orography simulations.

Surprisingly, the wave disturbance is rather different at higher altitudes. At 25 km. the wavevector is aligned in the NE-SW direction, apparently the wavevector is rotating with altitude (Fig. not shown). This could be explained by the refraction suffered by the waves due to the strong horizontal shear in the region, but also there may be an evidence of wave filtering, since the surface wind is rotating and also is transitory, then we expect a broad spectrum in both frequency and wavenumber, if some of their components are filtered in low heights, a different wavevector will be dominant in higher altitudes (e.g. Broad, 1999).

A longitude-height cross-section of the horizontal wind strength $(u^2+v^2)^{1/2}$ is shown in Fig. 11 at 50S, the place where the highest mountains are located. On 10/30 between 00:00 and 6:00 hours strong surface winds are developing. These strong winds in the region are a result of the eastward propagation of a synoptic wave, when the negative phase in meridional wind arrives to the mountain range, the gravity wave disturbances are triggered (Fig. 12).

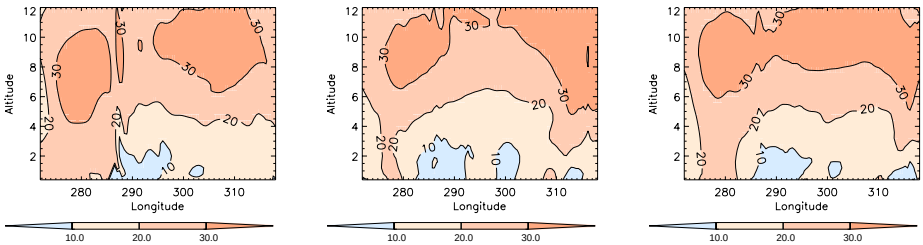

Figure 11: Wind strength at 50S (latitude of the highest mountain. The panels are showing the moment of the wave generation, 10/29 18:00 (left panel) 10/30 00:00 (middle panel) and 10/30 06:00 (right panel).

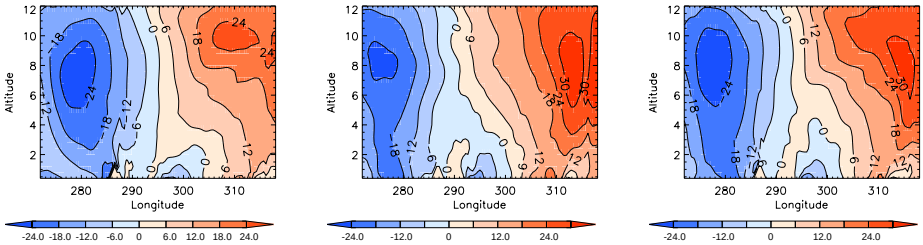

Figure 12: As Fig. 11 but meridional wind.

3.2 Evidence of critical levels and wave breaking

The measurements made by the radiosonde launched on 11/1 suggest the presence of instabilities which could be produced by the wave perturbations, and therefore the wave could be breaking. Figure 12 shows the wind field at 20 hPa (~26 km), the field is almost purely rotational centred in the region of the disturbance, there is a small wind strength and the wind vector is perpendicular to the wave vector. This suggests the presence of critical levels for the main components of the spectral distribution (in low heights the wind is rotating because of the synoptic wave propagation so a broad range of wave components are generated).

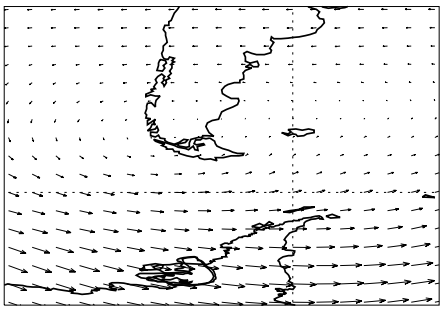

Figure 13 Wind vector at 20mb on 11/1 18:00 from ERA40 data. Note that flow is perpendicular to wave vector. Besides amplitude is very small, suggesting the presence of critical levels.

Figure 14 shows a x-z cross-section of the potential temperature located at 54S, the wave is strongly perturbating the potential temperature and is producing the classical picture of wave overturning, with an important potential temperature discontinuity at about 22 km. Above it, the disturbance is strongly damped or it is unable to reach higher altitudes than the critical level. The wave-induced perturbations in the temperature potential are producing a convective instability in the flow. The observations do not show a convective instability but a dynamical instability at 25 km, however the overturning height in the simulation depends strongly on the wave phase, location and time, in general we found that the flow is overturning in a height interval from 15 km to 25 km. An explanation of the overturning height dependence with location is that the zero zonal wind surface depends on latitude, the height of the zero zonal wind is 24 km at 50S and 30 km at 54S and is descending with time.

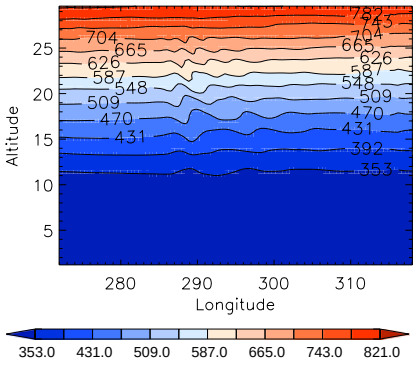

Figure 14. Cross-section of potential temperature perturbations at -54 South (x-z). The figure suggests the possibility of wave breaking trough overturning.

4. DISCUSSION

We have found very high wave energy episodes at Ushuaia (Argentina). The wave events have been shown to be connected with The Andes mountain range and the strong surface winds observed in the Patagonia region. These wave events reach wave wind amplitudes of 10 m/s in the lower stratosphere. In particular, the case study appears to be triggered by the passage (downstream propagation) of a baroclinic wave through the Andes mountains.

The ``orographic'' wave packets propagate in the southeast direction for a quite long way. Indeed they reach the Antarctic peninsula and Georgia islands region on 11/3. The horizontal wavelength ranges 400~km to 700~km and appears to be changing with time and distance to the mountain. The disturbance persists for an exceptionally long time, as observed with the radiosondes and confirmed with the WRF simulations, the disturbance starts developing on 10/30 and still is present on 11/1. The WRF simulations show that the high activity disturbance remains for 60 hours, although modulations of the wave amplitude are found in that period.

Since a baroclinic wave is developing and propagating slowly toward the East, there is a possibility that the waves were generated by geostrophic adjustment. However, this possibility is rejected through a simulation with the same initial and boundary conditions but without orography that shows no disturbances in the region. On the other hand, the baroclinic wave appears to be instrumental in the triggering of the orographic waves.

The perturbation in the stratosphere exhibits characteristics of inertia-gravity waves, the meridional and zonal components are out of phase and the hodograph presents an ellipse. The interpretation of these waves as being produced by temporal dependence of the mean flow (Cornish and Larsen, 1989), height dependence of the mean flow or geostrophic adjustment of the orographically perturbed flow (Scavuzzo, *et al.*, 1998) are

all feasible in the observed flow conditions. Further analysis will focus on finding out the interpretation that adjust to the case study.

Acknowledgements.
We thank to the European Center for Medium Weather Forecasts (ECMWF) and the Centre National d'Etudes Spatiales (CNES) for providing the data used in this work.

BIBLIOGRAPHY

Broad, A., 1999. Do orographic waves break in flows with uniform wind direction turning with height?. *Q. J. R. Meteorol. Soc.*, **125**, 1695-1714.

Cornish C. R. and M. F. Larsen, 1989: Observations of low-frequency inertia-gravity waves in the lower stratosphere over Arecibo. *J. Atmos. Sci.*, **46**, 2428-2439.

Charney, J., 1947. The dynamics of long waves in a baroclinic westerly current. *J. Meteor.*, **4**, 135-162.

Garcia, R. R. and B. A. Boville, 1994. Downward control of the mean meridional circulation and temperature distribution of the polar winter stratosphere. *J. Atmos. Sci.*, **51**, 2238-2245.

Hines, C. O., 1989. Tropopausal mountain waves over Arecibo: A case study. *J. Atmos. Sci.*, **46**, 476-488.

Holton, J. R., 1992. *An introduction to dynamic metereology*. Academic Press, 3rd edition.

McIntyre M. E., 1989. On the Antarctic ozone hole. *J. Atmos. and Terr. Phys.*, **51**, 29-43.

Orlanski, I., and J. J. Katzfey, 1991: The life cycle of a cyclone wave in the Southern Hemisphere. Part I: Eddy energy budget. *J. Atmos. Sci.*, **48**, 1972-1998.

O'Sullivan D. and T. Dunkerton, 1995. Generation of inertia-gravity waves in a simulated life cycle of baroclinic instability, *J. Atmos. Sci.*, **52**, 3695-3716.

Pierce, R. B. and coauthors, 1994. Mixing processes within the polar night jet. *J. Atmos. Sci.*, **51**, 2957-2972.

Plougonven, R. and H. Teitelbaum, 2003. Comparison of a large-scale inertia-gravity wave as seen in the ECMWF analyses and from radiosondes. *Geophys. Res. Lett.*, **30**, 1954, doi:10.1029/2003GL0177716.

Scavuzzo, C. and M. Lamfri and H. Teitelbaum and F. Lott, 1998. A study of the low-frequency inertio-gravity waves observed during PirEx. *J. Gheophys. Res.*, **103**, 1747-1758.

Trenberth K. E., 1991: Storm Tracks in the Southern Hemisphere. *J. Atmos. Sci.*, **48**, 2159-2178.

Uccellini L. and S. Koch, 1987. The synoptic setting and possible energy sources for mesoscale wave disturbances. *Mon. Wea. Rev.*, **115**, 721-729.

Zhang, F., 2004. Generation of mesoscale gravity waves in upper-tropospheric jet-front systems. *J. Atmos. Sci.*, **61**, 440-457.